Rapid Communications

Length scale for magnon-polaron formation from nonlocal spin transport

Babak Zare Rameshti[1] and Rembert A. Duine[2,3]

[1]*Department of Physics, Iran University of Science and Technology, Narmak, Tehran 16844, Iran*

[2]*Institute for Theoretical Physics, Utrecht University, Princetonplein 5, 3584 CC Utrecht, The Netherlands*

[3]*Department of Applied Physics, Eindhoven University of Technology, P.O. Box 513, 5600 MB Eindhoven, The Netherlands*

(Received 24 July 2018; revised manuscript received 16 November 2018; published 7 February 2019)

We develop a theory for nonlocal spin transport through magnetic insulators that treats the coherent magnetoelastic interaction on equal footing with incoherent relaxation processes. In particular, our theory is able to describe the formation of magnon polarons, hybridized spin and elastic waves, near an interface where spin is injected into the magnetic insulator. Our theory is based on the stochastic Landau-Lifshitz-Gilbert equation coupled to stochastic equations of motion for the lattice displacement. By solving these equations, we obtain the charge voltage generated in a detector on one side of the magnetic insulator in response to spin biasing with an injector on the other side. We find that though magnon-polaron formation causes anomalous features in the spin transport, a length scale exists, however, below which magnetoelastic coupling does not affect the nonlocal spin current. This finding may motivate experiments to explore this aspect of magnon-phonon coupling in magnetic materials.

DOI: 10.1103/PhysRevB.99.060402

Introduction. Lattice distortions can affect spin waves within a magnet due to magnetoelastic coupling (MEC). The dynamics of phonons, the quanta of lattice distortions, is likewise influenced by magnons, the quanta of spin waves. The MEC leads to magnon polarons (MPs), i.e., coherently hybridized quasiparticles that form near the anticrossing of the uncoupled magnetic and acoustic dispersions [1]. This hybridized state has been reconsidered very recently in the magnetic insulator yttrium iron garnet (YIG) [2–5]. This material allows one to access the strong-coupling regime due to its unique acoustic and magnetic quality. In this regime the rate for coherent energy exchange exceeds the dissipative loss rates. The interconversion between magnons and phonons via MEC can be detected in various experimental setups such as magneto-optical [3,6] and transport [7] measurements.

The spin and thermal transport properties of magnetic insulators are altered by the resonant coupling of magnons and phonons. The signature of this resonant coupling has been found in several transport experiments, such as the spin Seebeck effect [8] and the spin Peltier effect [9]. It has been observed that MEC can lead to a resonant enhancement of the local spin Seebeck effect [4], where a thermal gradient drives a magnon spin current through the magnetic insulator. While these local transport measurements thus provide insights on the magnon-phonon interaction, we focus in this Rapid Communication on a nonlocal spin transport setup which, as we shall show, provides additional information on the formation of MPs.

Generally, nonlocal spin transport experiments are able to probe the transport properties of spin carriers not only in metals [10] and semiconductors [11], but also in magnetic insulators [12], where magnons act as information and energy carriers. Nonlocal spin transport schemes have proven useful in elucidating the transport features of magnons in YIG [13] that cannot be probed by a local configuration. Recently, nonlocal magnon spin transport devices have been used to address not only the generation but also the transport properties of MPs in YIG [14], showing that the nonlocal spin Seebeck signals in YIG|Pt bilayers are suppressed rather than enhanced due to the MP resonances.

Previous works concerning transport have thus focused on the influence of MPs on the local [4,5] and nonlocal spin Seebeck effect [14]. In this Rapid Communication, we point out that a nonlocal spin transport experiment probes the length scale for MP formation that is not straightforwardly extracted from spin Seebeck effect measurements. This length scale comes about because in a nonlocal setup the spin that is injected near the interface enters the magnon system only. For MPs to play a role in the nonlocal spin transport, the injector-detector distance needs to be larger than the MP formation length scale. This is reminiscent of a normal metal|superconductor bilayer in which the superconductivity is induced only over the superconducting coherence length, the length scale over which Cooper pairs can penetrate into the normal metal from the adjacent proximity coupled superconductor. Another example is the absorption, over a small length, of spin injected into a metallic magnet that has polarization transverse to the local magnetization direction [15].

To theoretically address the length scale for MP formation, we present a theory based on the stochastic Landau-Lifshitz-Gilbert equation [16] coupled to stochastic equations of motion for the lattice displacement. We determine the inverse spin Hall voltage drop in the detector in linear response to a spin accumulation, $\boldsymbol{\mu} = \mu\mathbf{z}$, generated in the injector by the spin Hall effect. We recover the anomalous features in the spin current related to MP formation that manifest themselves as peaks or dips in the spin current as a function of field. Moreover, we indeed find that these features disappear for

short injector-detector distances, indicating a length scale over which the MP forms. The theoretical description of this formation requires the inclusion of both incoherent and coherent dynamics which our formalism includes straightforwardly, but may be more cumbersome to incorporate in the Boltzmann approach of Ref. [5].

Model and formalism. The minimal model Hamiltonian that describes the coupling between elastic waves and magnetization in magnetic insulators reads

$$\mathcal{H} = \mathcal{H}_{\rm el} + \mathcal{H}_{\rm mag} + \mathcal{H}_{\rm MEC}. \tag{1}$$

Here, a cubic unit cell with spatially constant magnetization is considered for a magnetic insulator with the equilibrium saturation magnetization M_0 along the applied magnetic field H. The magnetization Hamiltonian $\mathcal{H}_{\rm mag}$ consists of linearized Zeeman $\mathcal{H}_Z$, and exchange $\mathcal{H}_{\rm ex}$ energies,

$$\mathcal{H}_Z = \mu_0 H M_0 \left(m_x^2 + m_y^2\right)/2, \tag{2a}$$

$$\mathcal{H}_{\rm ex} = A_{\rm ex}[(\nabla m_x)^2 + (\nabla m_y)^2], \tag{2b}$$

where m_x and m_y are the transverse components of the magnetization vector $\mathbf{m} = \mathbf{M}/M_0$, and $A_{\rm ex}$ denotes the exchange parameter. The lattice dynamics in an isotropic solid, with both kinetic and elastic contributions, is given by $\mathcal{H}_{\rm el} = (\rho/2)\dot{\mathbf{R}}\cdot\dot{\mathbf{R}} + (\lambda/2)(\sum_i S_{ii})^2 + \mu\sum_{ij} S_{ij}^2$, with $S_{ij} = (\partial_i R_j + \partial_j R_i)/2$ denoting the components of the strain tensor, ρ the mass density, λ and μ elastic constants, and where $\mathbf{R}$ represents the small displacements from an equilibrium state. The lowest-order expression for the MEC, satisfying the underlying symmetry, reads $\mathcal{H}_{\rm MEC} = \sum_{ij=x,y}(b + a\delta_{ij})S_{ij}m_i m_j + 2b\sum_{i=x,y} S_{ix}m_i$, where a and b are phenomenological magnetoelastic coupling coefficients.

We consider a magnetic insulator sandwiched between two heavy metal (Pt) contacts, as the injector and detector, with interfaces located along the planes $x = 0$ and $x = d$, which is translationally invariant in the yz plane (see Fig. 1). The system is driven out of equilibrium by a spin accumulation $\boldsymbol{\mu} = \mu\mathbf{z}$ maintained in the left lead by, e.g., the spin Hall effect [17]. At nonzero temperatures, the adequate treatment of the dynamics of the magnetization driven by thermal fluctuations requires that bulk and boundary fluctuations and losses of both magnons and phonons be considered in the equations of motion. The lattice displacement vector may be recast into the form of longitudinal R_l, in-plane transverse R_t and out-of-plane transverse R_y modes. The small amplitude excitations of coupled magnetization and lattice dynamics, $\Psi = (m_x, m_y, R_l, R_t, R_y)^{\rm T}$, are governed by the linearized coupled equation of motion in the bulk,

$$\mathscr{L}_{\rm B}\Psi = \mathfrak{h}_{\rm B}. \tag{3}$$

Here, $\mathscr{L}_{\rm B}$ denotes the bulk differential operator that follows from the coupled magnetoelastic equations of motion given in the Supplemental Material [18], while $\Psi = \Psi(x, \mathbf{q}, \omega)$ is the Fourier transform of the displacement vector. The stochastic force $\mathfrak{h}_{\rm B} = (\mathfrak{h}_{m_x}, \mathfrak{h}_{m_y}, \mathfrak{h}_{R_l}, \mathfrak{h}_{R_t}, \mathfrak{h}_{R_y})^{\rm T}$, that describes thermal agitation due to nonequilibrium magnetization and lattice noise in the bulk, is related to the Gilbert damping α and phonon relation time τ_p by the fluctuation dissipation

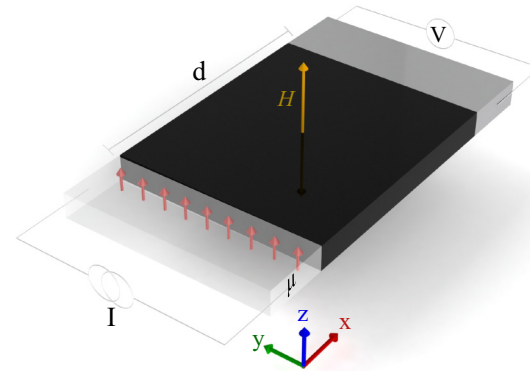

FIG. 1. Nonlocal spin transport configuration comprising a Pt|YIG|Pt heterostructure as a model system: A charge current I through the left Pt builds up a nonequilibrium spin accumulation $\boldsymbol{\mu} = \mu\mathbf{z}$ at the left Pt|YIG interface (injector) via the spin Hall effect. With MEC being present, the angular momentum is transferred, through the exchange interaction at the interface, to the excitations with a mixed character; magnon polaron. The diffusing MPs through the magnetic insulator induce a spin accumulation in the right Pt|YIG interface, which is used to be detected as a nonlocal charge voltage V in the detector, through the inverse spin Hall effect. The magnetization is saturated along the $\mathbf{z}$ axis by a magnetic field H. The injector-detector distance d, electrical injection, and detection schemes are indicated schematically.

theorem,

$$\langle \mathfrak{h}_i(x, \mathbf{q}, \omega)\mathfrak{h}_j(x', \mathbf{q}', \omega')\rangle = (2\pi)^3\delta_{ij}\eta_i\hbar\omega\frac{\delta(x - x')\delta(\mathbf{q} - \mathbf{q}')\delta(\omega - \omega')}{\tanh[\hbar\omega/2k_B T_i]}, \tag{4}$$

where $\eta_{1,2} = s\alpha$, with $s = M_0/\gamma$ being the saturated spin density, $\eta_{3,4,5} \sim \tau_p$ are generalized damping coefficients associated with lattice dynamics, and $k_B T_i$ is the local thermal energy associated with magnons and phonons.

The boundary conditions on Ψ at the two interfaces, considering both stochastic and deterministic spin-transfer torques, read

$$\mathscr{L}_{\rm L}\Psi = \mathfrak{h}_{\rm L} \quad (x = 0), \tag{5a}$$

$$\mathscr{L}_{\rm R}\Psi = \mathfrak{h}_{\rm R} \quad (x = d), \tag{5b}$$

in which $\mathscr{L}_{\rm L(R)}$ represents the interface operator for the left (right) boundary, which acts on Ψ, and $\mathfrak{h}_{\rm L(R)}$ corresponds to spin and phonon fluctuations in the normal lead at the left (right) interface. The spin current noise and lattice fluctuations in the normal metal lead to stochastic surface forces $\mathfrak{h}_{\rm L(R)}$ which relate to generalized damping coefficients η' according to the fluctuation-dissipation theorems for the $l = L, R$ interfaces,

$$\langle \mathfrak{h}_{1,i}(\mathbf{q}, \omega)\mathfrak{h}_{1',j}(\mathbf{q}', \omega')\rangle = (2\pi)^3\delta_{ll'}\delta_{ij}\eta'_i(\hbar\omega - \mu_{l,i})\frac{\delta(\mathbf{q} - \mathbf{q}')\delta(\omega - \omega')}{\tanh[(\hbar\omega - \mu_{l,i})/2k_B T_{l,i}]}, \tag{6}$$

where $\eta'_{1,2} = g^{\uparrow\downarrow}/4\pi$, with the interfacial spin mixing conductance $g^{\uparrow\downarrow}$, and $\eta'_{3,4,5} \equiv \eta'_p$, describing dissipation due to

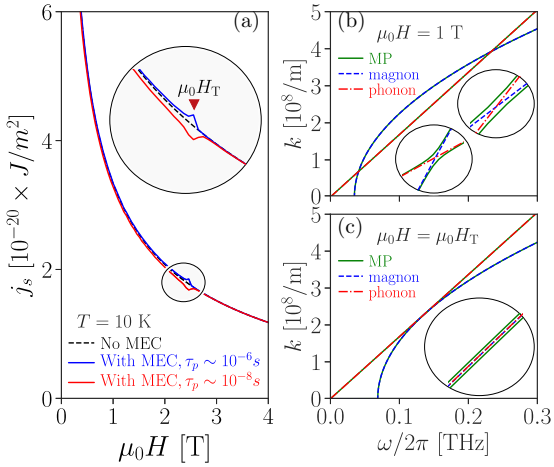

FIG. 2. (a) Magnetic field dependence of the nonlocal spin voltage j_s for two values of phonon relaxation times, $\tau_p \sim 10^{-6}$, 10^{-8} s [19], at an injector-detector distance of $d = 5$ μm, and $T = 10$ K. The material parameters of YIG are adopted here; saturation magnetization $M_0 = 1.4 \times 10^5$ A/m, magnetoelastic coupling $b = 6.96 \times 10^5$ J/m^3, exchange stiffness $D_{ex} = 2\gamma A_{ex}/M_0 = 8.2 \times 10^{-6}$ m^2/s, gyromagnetic ratio $\gamma/2\pi = 2.8 \times 10^{10}$ Hz/T, mass density $\rho = 5170$ kg/m^3, elasticity constant $\mu = 7.4 \times 10^{10}$ Pa, transverse sound velocity $c_t = 3.8 \times 10^2$ m/s, and Gilbert damping $\alpha = 10^{-4}$. The peak and dip in the signal correspond to $\mu_0 H = \mu_0 H_T \sim 2.5$ T, where the magnon-polaron formation is enhanced. The inset in (a) shows a closeup around the touching field. Magnon-polaron (MP), magnon, and transverse phonon dispersions are indicated in the right panels. (b) For $H < H_T$, the transverse phonon and magnon dispersions intersect at two points where magnetoelastic coupling is maximized (see insets), while (c) for the touching field $H = H_T$, the magnon and phonon dispersions become tangential to each other where the MP phase space formation is enlarged (see inset).

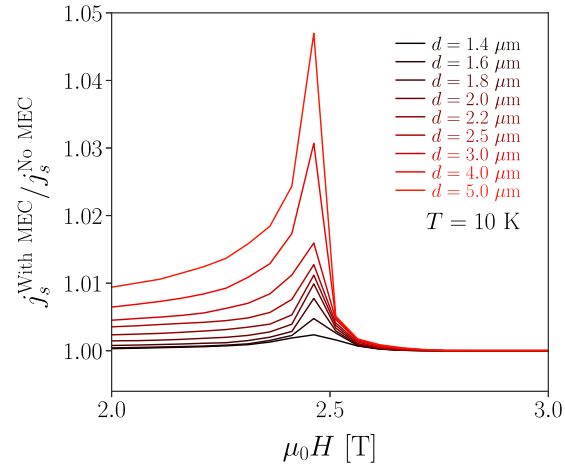

FIG. 3. The normalized nonlocal spin voltage $j_s^{\text{With MEC}}/j_s^{\text{No MEC}}$ as a function of magnetic field for varying injector-detector distances d from 1.4 to 5.0 μm at $T = 10$ K. The peaks correspond to $\mu_0 H \sim 2.5$ T, where phonon and magnon dispersions become tangential to each other which maximizes the phase space of MP formation. The MP peak disappears for short lengths, indicating a length scale over which the MP forms.

the spin pumping and interfacial phonon fluctuations, respectively, at the interfaces. In our setup, $\mu_{l,1,2} = \mu_{l,m}$ (with $\mu_{L,m} = \mu$, and $\mu_{R,m} = 0$) and $\mu_{l,3,4,5} = \mu_p = 0$ denote the spin and phonon accumulation in the leads while $T_{l,1,2} = T_m$ and $T_{l,3,4,5} = T_p$ are their corresponding temperatures, respectively. We assume a large phononic heat conductance through the system and good thermal contact at the interfaces. Moreover, we treat the normal metal layers as perfect spin sinks, so that any spin accumulation generated by spin pumping is quickly relaxed, which allows neglecting the back flow to metallic leads from magnetization dynamics in the magnetic insulator, thus resulting in a net spin current across the right YIG|Pt interface.

The coupled magnetic and lattice dynamics in the magnetic insulator can be determined by the equation of motion in the bulk [Eq. (3)], along with the boundary conditions [Eqs. (5)], in which metallic leads serve as a thermal noise bath for both magnetic and elastic degrees of freedom. Here, only the average ensemble information of the noise, provided in Eqs. (4) and (6), is required.

Magnon-polaron transport. The generated spin current, due to the nonequlibrium state at the interface of the left normal metal|magnetic insulator, can be detected nonlocally by the inverse spin Hall effect as shown in Fig. 1. The thermally averaged spin current with spin polarization in the z direction flowing through the right interface at $x = d$, in linear response to the driving force $\boldsymbol{\mu} = \mu \mathbf{z}$ at the left interface, is given by

$$j_s \equiv \langle \mathbf{z} \cdot \mathbf{j} \rangle = 2A_{ex} \langle m_y \partial_x m_x - m_x \partial_x m_y \rangle$$
$$= 2A_{ex} \langle \Psi_2(x) \partial_x \Psi_1(x) - \Psi_1(x) \partial_x \Psi_2(x) \rangle. \quad (7)$$

This may be recast into the form $j_s = G\mu$ by retaining terms only up to linear order in μ and introducing the spin conductance G. We focus mainly on spin waves propagating perpendicular to the external magnetic field, i.e., $\theta = \pi/2$, which couple only with the transverse acoustic modes R_t, due to symmetry. The assumption of one-dimensional transport is valid because the YIG thickness, along the $\mathbf{z}$ direction, is much smaller, typically a few hundred of nm, than the injector-detector separation distance d.

In Fig. 2(a), the nonlocal spin signal j_s as a function of magnetic field for different values of phonon relaxation times τ_p, an injector-detector distance of $d = 5$ μm, and $T = 10$ K, is shown. Without MEC, the spin current flowing through the right interface decreases monotonically with increasing magnetic field as magnons are frozen out by the magnetic field, while MEC leads to resonant features that appear close to the touching field $\mu_0 H_T = c_t^2/4D_{exc}\gamma \sim 2.5$ T (see Fig. 2), as the phase space of MP coupling is then maximal [4,14]. When the quality of the phonon transport channel is better than the magnon one, the hybridization of magnons with phonons provides a less diffusive transport channel for magnons which leads to an enhanced nonlocal spin current, while the suppressed spin current by the MEC is attributed to low-quality acoustics.

The spin current injected into the detector is calculated at $T = 10$ K and shown as a function of magnetic field around the anomaly and for various injector-detector distances in Fig. 3. The nonlocal signal in the presence of MEC is normalized with the corresponding signal without MEC to

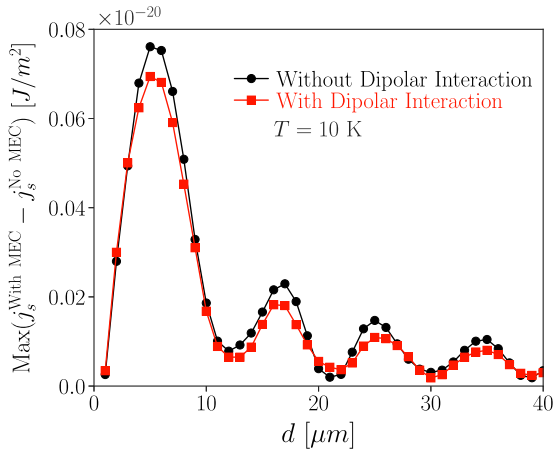

FIG. 4. The peak of magnon-polaron contribution with/without dipolar interactions to the nonlocal spin voltage, $\mathrm{Max}(j_s^{\text{With MEC}} - j_s^{\text{No MEC}})$, as a function of injector-detector distance at $T = 10$ K. The magnon-polaron contribution to the spin transport indicates a decaying oscillatory behavior as a function of thickness.

highlight the MP contribution to the magnon spin current. At small magnetic fields, where phonon and magnon dispersions intersect, the MEC strongly enhances the magnon spin current flowing across the right interface, due to the dressing of magnons by phonons with a larger group velocity. At higher magnetic fields, where phonon and magnon dispersions do not intersect, the MEC no longer influences the flow of spin current.

The nonlocal spin signal is calculated for various injector-detector distances d, to extract the length scale associated with the MP transport. Figure 3 clearly shows that the MP peak disappears for short lengths, revealing that a length scale over which MPs form is involved. The MP formation length scale below which the MP peak in the nonlocal spin signal disappears is approximately given by $\xi_{\text{MEC}} \sim \hbar v_g^{\text{MEC}}/\Delta_{\text{MEC}}$, where $v_g^{\text{MEC}} = \partial_k \omega(k)$ is the group velocity of the resulting MP, with $\omega(k)$ being the corresponding dispersion relation, and where Δ_{MEC} denotes the bare gap between magnons and phonons. This expression is motivated by the fact that the coherent superposition of the magnon and phonon will precess at a rate $\Delta_{\text{MEC}}/\hbar$ which determines its dephasing, and, together with the velocity v_g^{MEC}, defines the length scale. Inserting the YIG parameters, we find that $\xi_{\text{MEC}} \sim 1\ \mu$m, in agreement with the numerical results. The spin accumulated at the left interface is mostly injected into the magnon transport channel which needs to propagate over this length scale until the MP channel, formed in the bulk of the magnetic insulator, becomes accessible for spin transport. For distances shorter than the MP formation length, i.e., short junctions $d < \xi_{\text{MEC}}$, the lattice deformations and MEC thus have no effect on the spin transport.

Interestingly, the peak of the magnon-polaron contribution to the nonlocal spin voltage, $\mathrm{Max}(j_s^{\text{With MEC}} - j_s^{\text{No MEC}})$, shows a decaying oscillatory behavior as a function of injector-detector distance (Fig. 4) due to the interference of the MP wave function with its reflection at the right boundary of the magnetic insulator. This is reminiscent of an Fulde-Ferrell-Larkin-Ovchinnikov (FFLO)-like state generated in a ferromagnet|superconductor bilayer, which results in the oscillation of the induced superconducting pairing wave function as a function of the ferromagnet layer thickness. Here, the short-wavelength limit of the dipolar interaction, $\mathcal{H}_{\text{dip}} \approx (\mu_0 M_0^2) m_x^2 \sin^2\theta$, is adopted. The dipolar interaction is responsible for the anisotropy in the magnon dispersion, which appears in the distance dependence of the spin current.

Conclusion and discussion. We have developed a nonlocal MP spin transport theory in magnetic insulators, showing that magnetoelastic coupling can affect magnon spin transport above a specific length scale. Above this length, an anomalous peak structure appears in the nonlocal spin voltage as a function of field, for fields around the touching field. In our treatment, we have not included the coupling between the spin of the electrons in the Pt to the phonon spin in the YIG across the interface, which we expect to be weak. Future work should investigate the validity of this assumption, as well as the role of disorder.

Finally, we mention that the experimental results of Cornelissen *et al.* are consistent with our findings. Although the MP-related resonant feature at the touching field is clearly resolved in the signal due to the thermal magnon generation which can be measured in the second-harmonic response, it is hardly observed, however, in the nonlocal electrically generated signal, detected from the first-harmonic response. This could be because the injector-detector separation distances are already below or comparable to the MP formation length scale. We hope that our results motivate experiments to further explore the proposed length scale for MP formation.

Acknowledgments. We thank S. A. Bender for fruitful discussions. B.Z.R. thanks the Institute for Research in Fundamental Sciences (IPM), where part of this work has done, for their support. This research was supported by the Iran Science Elites Federation (B.Z.R.). This work is part of the research program of the Foundation for Fundamental Research on Matter (FOM) via the program Magnon Spintronics FOM-159, which is part of the Netherlands Organisation for Scientific Research (NWO).

[1] C. Kittel, Phys. Rev. **110**, 836 (1958); E. Schlömann, J. Appl. Phys. **31**, 1647 (1960).

[2] A. Rückriegel, P. Kopietz, D. A. Bozhko, A. A. Serga, and B. Hillebrands, Phys. Rev. B **89**, 184413 (2014); N. Ogawa, W. Koshibae, A. J. Beekman, N. Nagaosa, M. Kubota, M. Kawasaki, and Y. Tokura, Proc. Natl. Acad. Sci. U.S.A. **112**, 8977 (2015); A. Kamra, H. Keshtgar, P. Yan, and G. E. W. Bauer, Phys. Rev. B **91**, 104409 (2015); S. C. Guerreiro and S. M. Rezende, *ibid.* **92**, 214437 (2015); H. Man, Z. Shi, G. Xu, Y. Xu, X. Chen, S. Sullivan, J. Zhou, K. Xia, J. Shi, and P. Dai, *ibid.* **96**, 100406(R) (2017).

[3] K. Shen and G. E. W. Bauer, Phys. Rev. Lett. **115**, 197201 (2015).

[4] T. Kikkawa, K. Shen, B. Flebus, R. A. Duine, K. I. Uchida, Z. Qiu, G. E. W. Bauer, and E. Saitoh, Phys. Rev. Lett. **117**, 207203 (2016).

[5] B. Flebus, K. Shen, T. Kikkawa, K. I. Uchida, Z. Qiu, E. Saitoh, R. A. Duine, and G. E. W. Bauer, Phys. Rev. B **95**, 144420 (2017).

[6] A. V. Scherbakov, A. S. Salasyuk, A. V. Akimov, X. Liu, M. Bombeck, C. Brüggemann, D. R. Yakovlev, V. F. Sapega, J. K. Furdyna, and M. Bayer, Phys. Rev. Lett. **105**, 117204 (2010); J.-W. Kim, M. Vomir, and J.-Y. Bigot, *ibid.* **109**, 166601 (2012); J. V. Jäger, A. V. Scherbakov, B. A. Glavin, A. S. Salasyuk, R. P. Campion, A. W. Rushforth, D. R. Yakovlev, A. V. Akimov, and M. Bayer, Phys. Rev. B **92**, 020404(R) (2015).

[7] K. Uchida, H. Adachi, T. An, T. Ota, M. Toda, B. Hillebrands, S. Maekawa, and E. Saitoh, Nat. Mater. **10**, 737 (2011); M. Weiler, H. Huebl, F. S. Goerg, F. D. Czeschka, R. Gross, and S. T. B. Goennenwein, Phys. Rev. Lett. **108**, 176601 (2012).

[8] M. Agrawal, V. I. Vasyuchka, A. A. Serga, A. D. Karenowska, G. A. Melkov, and B. Hillebrands, Phys. Rev. Lett. **111**, 107204 (2013); M. Schreier, A. Kamra, M. Weiler, J. Xiao, G. E. W. Bauer, R. Gross, and S. T. B. Goennenwein, Phys. Rev. B **88**, 094410 (2013).

[9] J. Flipse, F. K. Dejene, D. Wagenaar, G. E. W. Bauer, J. Ben Youssef, and B. J. van Wees, Phys. Rev. Lett. **113**, 027601 (2014).

[10] F. J. Jedema, A. T. Filip, and B. J. van Wees, Nature (London) **410**, 345 (2001).

[11] X. Lou, C. Adelmann, S. A. Crooker, E. S. Garlid, J. Zhang, K. S. M. Reddy, S. D. Flexner, C. J. Palmstrøm, and P. A. Crowell, Nat. Phys. **3**, 197 (2007).

[12] L. J. Cornelissen, J. Liu, R. A. Duine, J. Ben Youssef, and B. J. van Wees, Nat. Phys. **11**, 1022 (2015).

[13] K. Ganzhorn, T. Wimmer, J. Cramer, R. Schlitz, S. Geprägs, G. Jakob, R. Gross, H. Huebl, M. Kläui, and S. T. B. Goennenwein, AIP Adv. **7**, 085102 (2017); L. J. Cornelissen, J. Shan, and B. J. van Wees, Phys. Rev. B **94**, 180402(R) (2016); L. J. Cornelissen and B. J. van Wees, *ibid.* **93**, 020403(R) (2016).

[14] L. J. Cornelissen, K. Oyanagi, T. Kikkawa, Z. Qiu, T. Kuschel, G. E. W. Bauer, B. J. van Wees, and E. Saitoh, Phys. Rev. B **96**, 104441 (2017).

[15] D. C. Ralph and M. D. Stiles, J. Magn. Magn. Mater. **320**, 1190 (2008).

[16] S. Hoffman, K. Sato, and Y. Tserkovnyak, Phys. Rev. B **88**, 064408 (2013).

[17] L. J. Cornelissen, K. J. H. Peters, G. E. W. Bauer, R. A. Duine, and B. J. van Wees, Phys. Rev. B **94**, 014412 (2016); S. S.-L. Zhang and S. Zhang, *ibid.* **86**, 214424 (2012).

[18] See Supplemental Material at http://link.aps.org/supplemental/10.1103/PhysRevB.99.060402 for a detailed derivation of the linearized equations of motion and boundary conditions.

[19] M. F. Lewis and E. Patterson, J. Appl. Phys. **39**, 1932 (1968).